Coherent streamflow variability in Monsoon Asia over the past eight centuries—links to oceanic drivers*

Hung T.T. Nguyen†[1], Sean W.D. Turner[2], Brendan M. Buckley[3], and Stefano Galelli[1]

[1]Pillar of Engineering Systems and Design, Singapore University of Technology and Design, Singapore
[2]Pacific Northwest National Laboratory, Washington, USA
[3]Lamont-Doherty Earth Observatory, Columbia University, NY, USA

Key points

- Climate-informed dynamic streamflow reconstruction is skillful over most of Monsoon Asia
- Spatial coherence of streamflow suggests water management be coordinated among basins
- Mekong and Chao Phraya are most sensitive among rivers to anomalies in sea surface temperature

Abstract

The Monsoon Asia region is home to ten of the world's biggest rivers, supporting the lives of 1.7 billion people who rely on streamflow for water, energy, and food. Yet, a synoptic understanding of multi-centennial streamflow variability for this region is lacking. Here we produce the first large scale streamflow reconstruction over Monsoon Asia (63 stations in 16 countries), using a novel climate-informed dynamic algorithm that is skillful over 92% of the gauging stations. We show that streamflow in Monsoon Asia is spatially coherent, owing to common drivers from the Pacific, Indian, and Atlantic Oceans that exert their greatest influence over the Mekong and Chao Phraya basins. This work increases our understanding of streamflow variability over Monsoon Asia. We suggest that future water management in the region should be coordinated between basins, taking into account the states of the oceans.

Plain Language Summary

Ten of the world's biggest rivers are located entirely within the Asian Monsoon region. They provide water, energy, and food for 1.7 billion people. To manage these critical resources, we need a better understanding of river discharge—how does it change over a long time? Are there common variation patterns among rivers? To answer these questions, we use information derived from tree rings to reconstruct river discharge history at 63 gauges in 16 Asian countries. Our reconstruction reveals the riparian footprint of megadroughts and large volcanic eruptions over the past eight centuries. We show that simultaneous droughts and pluvials have often occurred at adjacent river basins in the past, because Asian rivers share common influences from the Pacific, Indian, and Atlantic Oceans. We also show that the oceans exert their greatest influences on the Mekong and Chao Phraya basins. From these findings, we suggest that future water management in the region should be coordinated between basins, taking into account the states of the oceans. Our findings can benefit the riparian people of the Asian Monsoon region.

*This manuscript is under review with *Geophysical Research Letters*
†Corresponding author, tanthaihung_nguyen@mymail.sutd.edu.sg

1 Introduction

Of the world's 30 biggest rivers, ten are located within Monsoon Asia, and two others originate from this region (Figure 1). These river basins are home to 1.7 billion people (Best, 2019). With high population densities, even smaller basins support the livelihood of millions—e.g., Chao Phraya (Thailand): 25 million, Angat (the Philippines): 13 million, and Citarum (Indonesia): 10 million (Nguyen and Galelli, 2018; Libisch-Lehner et al., 2019; D'Arrigo et al., 2011). River discharge, or *streamflow*, provides water for domestic and industrial uses, irrigation, and hydropower. It sustains aquatic life (including fish yield), carries sediment and nutrients, and enables navigation. Streamflow is an important link in both the water-energy-food nexus and the ecological cycle. To manage this resource, we need a good understanding of hydrologic variability. Such understanding is often derived from streamflow measurements; however, these instrumental data span typically only a few decades, too short to capture long-term variability and changes in streamflow.

When compared against instrumental data, longer streamflow records reconstructed from climate proxies—such as tree rings—often reveal striking insights. A reconstructed pre-dam variability of the Yellow River (Li et al., 2019) shows that streamflow in 1968–2010 was only half of what should have been; in other words, dam-related activities depleted half of the available water! A reconstruction of the Citarum River (Indonesia) (D'Arrigo et al., 2011) shows that the period 1963–2006 contained an increasing trend of low flow years but no trend in high flow years, compared with the previous three centuries. This finding suggests that 10 million inhabitants of Jakarta may be facing higher drought risks than what is perceived from the instrumental record. The Mongolian "Breadbasket", an agricultural region in north-central Mongolia (Pederson et al., 2013), experienced an unusually wet twentieth-century, and the recent dry epoch is not rare in the last four centuries (Davi et al., 2006; Pederson et al., 2013; Davi et al., 2013). Consequently, agricultural planning cannot take the twentieth century to be the norm, lest history repeats the lesson of the Colorado River Basin: observations over abnormally wet years (Stockton and Jacoby, 1976; Woodhouse et al., 2006) led to water rights overallocation, and the Colorado no longer reaches the Pacific Ocean.

Compelling evidence calls for more streamflow reconstructions in Monsoon Asia. Tremendous efforts, booming in the last four years (Figure S1), have partly addressed this need, but the hydrological knowledge gained was limited to the individual catchments studied, more than half of which are in China (Text S1 and Table S1). A synoptic understanding is lacking. Here, we produce the first large scale streamflow reconstruction for Monsoon Asia, covering 63 stations in 16 countries, unraveling eight centuries of annual streamflow variability. Fifty-nine stations are reconstructed for the first time while the other four (Citarum, Yeruu, Ping, and Indus Rivers) are extended back in time compared to previous works (D'Arrigo et al., 2011; Pederson et al., 2013; Nguyen and Galelli, 2018; Rao et al., 2018). This data set allows us to assess both local historical water availability and regional streamflow patterns, revealing the spatial coherence of streamflow and its links to the oceans. This understanding may improve interbasin water resources management and coordination.

2 Data and Methods

2.1 Streamflow and Proxy Data

We obtained streamflow data from the Global Streamflow Indices and Metadata (GSIM) data set (Do et al., 2018; Gudmundsson et al., 2018), using stations having at least 41 years of data, with no more than 3% missing daily values, and with mean annual flow of at least 50 m^3/s. We also received streamflow data from our colleagues (see Acknowledgment). Our collection effort resulted in a data set of mean annual (January–December) flow at 63 stations in 16 countries (Figure 1). We used the calendar year as there is not a common water year across

the study domain (Knoben et al., 2018). We acknowledge that the instrumental data may contain anthropogenic effects such as those caused by reservoir operations. This is a common issue in streamflow reconstruction (Xu et al., 2019). Working with annual rather than seasonal streamflow ameliorates the effects of upstream reservoirs, which transfer water from wet season to dry season but have less impact on the annual water budget.

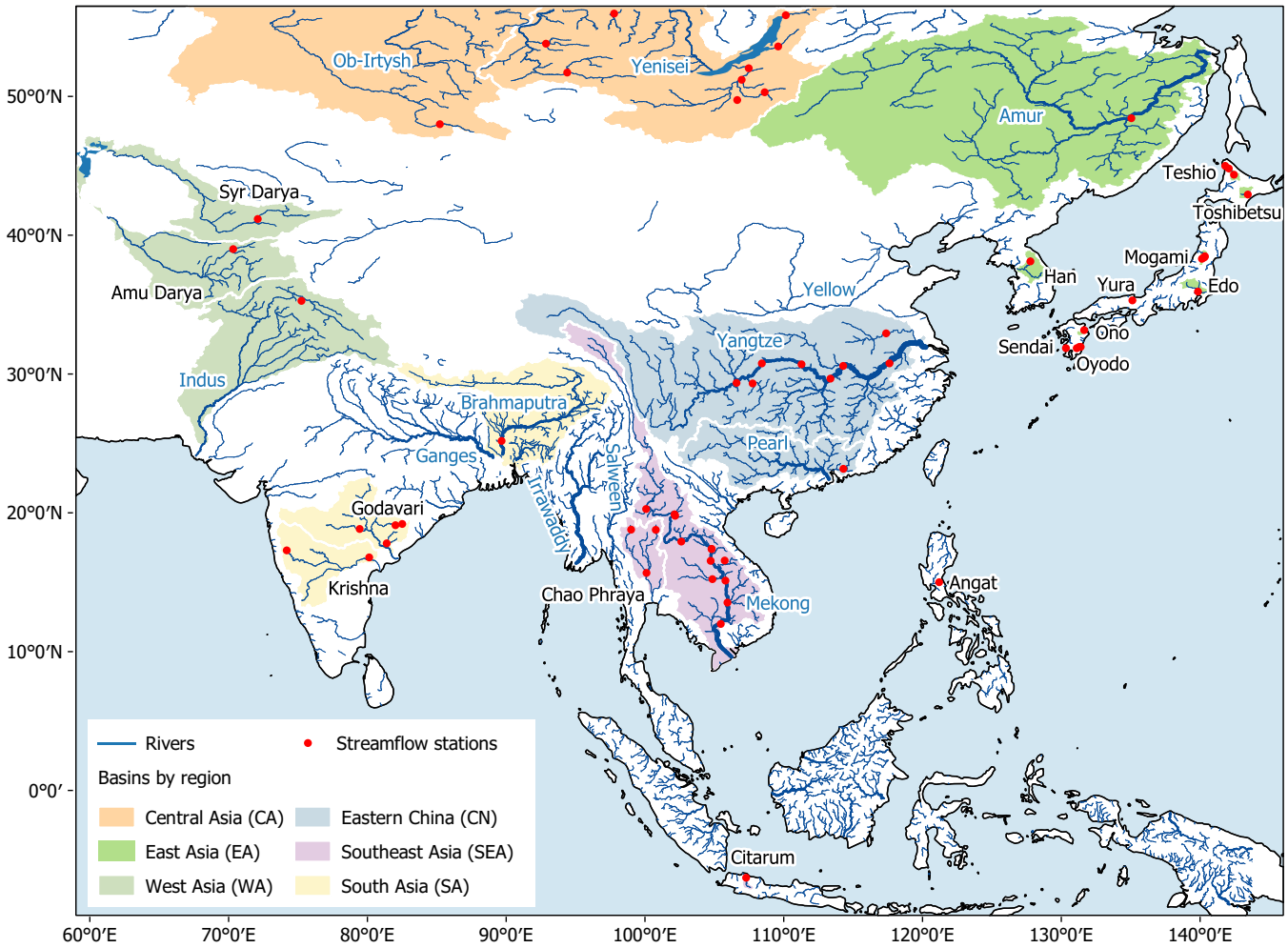

Figure 1. The Monsoon Asia region (Cook et al., 2010); river basins involved in this study are highlighted by sub-region, rivers belonging to the world's 30 biggest (Best, 2019) shown with blue names.

2.2 Climate-informed Dynamic Streamflow Reconstruction

Our paleoclimate proxy is the Monsoon Asia Drought Atlas (MADA) (Cook et al., 2010) version 2 (Cook, 2015), a gridded data set of the Palmer Drought Severity Index (PDSI) (Palmer, 1965) for the period 1200–2012, reconstructed from tree rings. Drought atlases have been shown to be a good climate proxy: since both streamflow and PDSI can be modeled as functions of ring width, one can build a model to relate streamflow to PDSI directly (Ho et al., 2016, 2017; Nguyen and Galelli, 2018). Drought atlases enhance the spatial expression of the underlying tree ring data, and are more uniform in space and time than the tree ring network itself (see Cook et al., 2010, Figure 1), making them better suited to large scale studies.

Our reconstruction method is based on the Point-by-Point-Regression (PPR) procedure (Cook et al., 1999, 2010; Cook, 2015). The premise behind PPR is that building a large-scale spatial regression model is challenging; therefore, one can reconstruct each target point (a climate

time series at a location) independently—hence the term point-by-point—and rely on the proxy network to capture the spatial patterns. Here, we adopted PPR, but with two key modifications: first, in the way proxy points are selected, and second, in the regression model.

The PPR procedure used for MADA (Cook et al., 2010) selected proxy points (tree ring chronologies) within a search radius, performed weighted Principal Component Analysis (PCA) on the selected points, and repeated for different radii and PCA weights. Given that geographical proximity does not imply hydroclimatic similarity, we selected our proxies (MADA grid points) by hydroclimatic similarity directly. The hydroclimate at location i (a MADA grid point or a streamflow station) is characterized by three indices: aridity a_i, moisture seasonality s_i, and snow fraction f_i, following Knoben et al. (2018) (hereafter referred to as the KWF system, after the three authors). The hydroclimatic similarity between two locations i and j is then defined as their Euclidean distance in the hydroclimate space. This distance is termed the KWF distance and its mathematical definition is

$$d_{KWF}(i,j) = \sqrt{(a_i - a_j)^2 + (s_i - s_j)^2 + (f_i - f_j)^2} \tag{1}$$

The KWF distance lets us screen out MADA grid points that are geographically close to the station of interest but hydroclimatically different—a climate-informed grid point selection scheme. Whereas previous PPR implementations varied the search radius, we fixed the radius to 2,500 km—the scale of regional weather systems (Boers et al., 2019)—and varied the KWF distance. In our search regions, PDSI often correlates significantly with streamflow (Figure S2); indeed hydroclimatic similarity is a physical basis for correlation. The final reconstruction ensemble includes 18 members as combinations of three different KWF distances and six PCA weights. Details of the procedure are described in Text S2.

The second step was to model the relationship between climatic inputs and the catchment output (streamflow). Here, this relationship was not modeled with linear regression (as with original PPR, and as typical with previous reconstruction studies), but as a linear dynamical system (LDS), following equations (2) and (3):

$$x_{t+1} = Ax_t + Bu_t + w_t \tag{2}$$

$$y_t = Cx_t + Du_t + v_t \tag{3}$$

where t is the time step (year), y the catchment output (streamflow, log-transformed to obtain a normal distribution), u the climatic input (an ensemble member from the climate-informed grid point selection), w and v white noise, and x the system state, which can be interpreted as the catchment's flow regime, i.e, wet or dry (Nguyen and Galelli, 2018). By modeling the flow regime and its transition, the LDS model accounts for both regime shifts (Turner and Galelli, 2016) and catchment memory (Pelletier and Turcotte, 1997). These behaviors are not modeled in linear regression.

Consistent with previous studies, we assessed reconstruction performance using the metrics Reduction of Error (RE) and Coefficient of Efficiency (CE) (Cook and Kairiukstis, 1990). We cross-validated individual stations with a leave-25%-out procedure with 100 repetitions and calculated the mean score of each metric. The reconstruction and cross-validation procedures were carried out using the R package *ldsr* (`github.com/ntthung/ldsr`).

3 Results and Discussion

3.1 Reconstruction Skills

Reduction of Error (RE) is positive at all stations (Figure 2a and b); Coefficient of Efficiency (CE) is positive at all but five (Figure 2c and d). Negative CE values belong in two distinct groups. Three stations in southern Japan may be affected by the low density in that segment of the tree ring network used to build the MADA (Cook, 2015); nevertheless, their CE values

are only slightly negative ($-0.063 < CE < 0$). On the other hand, stations Ban Mixay ($CE = -0.125$) and Ubon ($CE = -0.118$) are located in the Mekong tributaries, in the area of high quality tree ring chronologies (Buckley et al., 2007; Sano et al., 2009; Buckley et al., 2010), yet their variability is poorly captured by the MADA, in stark contrast with nearby stations. We suspect there are data errors at these two gauges. The negative CE values here are likely not due to the reconstruction model. The histogram of CE resembles that of RE but skews and shifts slightly left. This is expected as CE is a more stringent metric than RE (Cook and Kairiukstis, 1990). Much lower CE than RE implies overfitting; we do not observe that here.

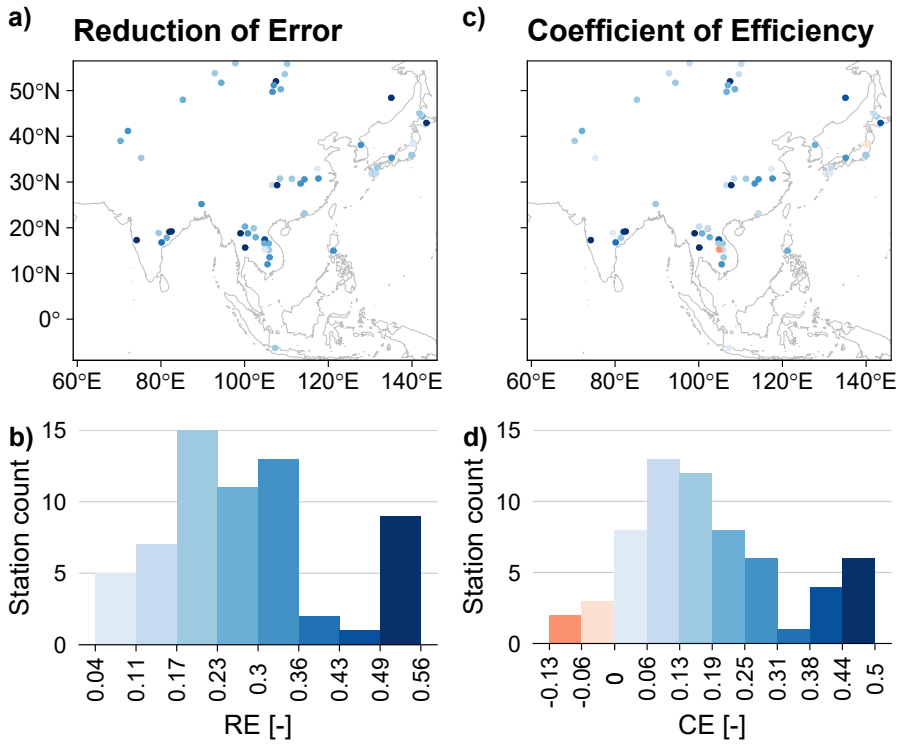

Figure 2. Distribution of model performance scores. Panels a and c show the scores of each station following the color legends encoded with the histograms in panels b and d.

3.2 Spatiotemporal Variability of Monsoon Asia's Streamflow

Both metrics have similar spatial distributions. Expectedly, lower (but positive) skills are seen in most of Central and West Asia, which lie outside the active monsoon area. An exception is the upper reach of the Selenge River (upstream of Lake Baikal), where model skill is remarkably high, owing to high quality tree ring records from Mongolia (Davi et al., 2006; Pederson et al., 2013; Davi et al., 2013; Pederson et al., 2014). In Japan, where the small catchments are sensitive to local climates, model skill is reduced. In all other regions, model skill is homogeneous. The consistent performance of our model suggests that anthropogenic changes have not affected the PDSI–streamflow relationship, the MADA is a good proxy for streamflow reconstruction in Asia, and our climate-informed dynamic reconstruction is skillful.

Having obtained good skill scores, we now present eight centuries of spatiotemporal streamflow variability in Monsoon Asia (Figure 3). This reconstructed history captures the riparian footprint of major historical events (large volcanic eruptions, megadroughts, and pluvials). We first discuss the impact of the three largest eruptions of the past eight centuries (Sigl et al., 2015): Samalas (1257) (Lavigne et al., 2013), Kuwae (1452-53) (Gao et al., 2006), and Tambora (1815) (Stothers, 1984).

Assuming that Kuwae erupted in 1452 (consistent with tree ring records, see e.g. Briffa et al.,

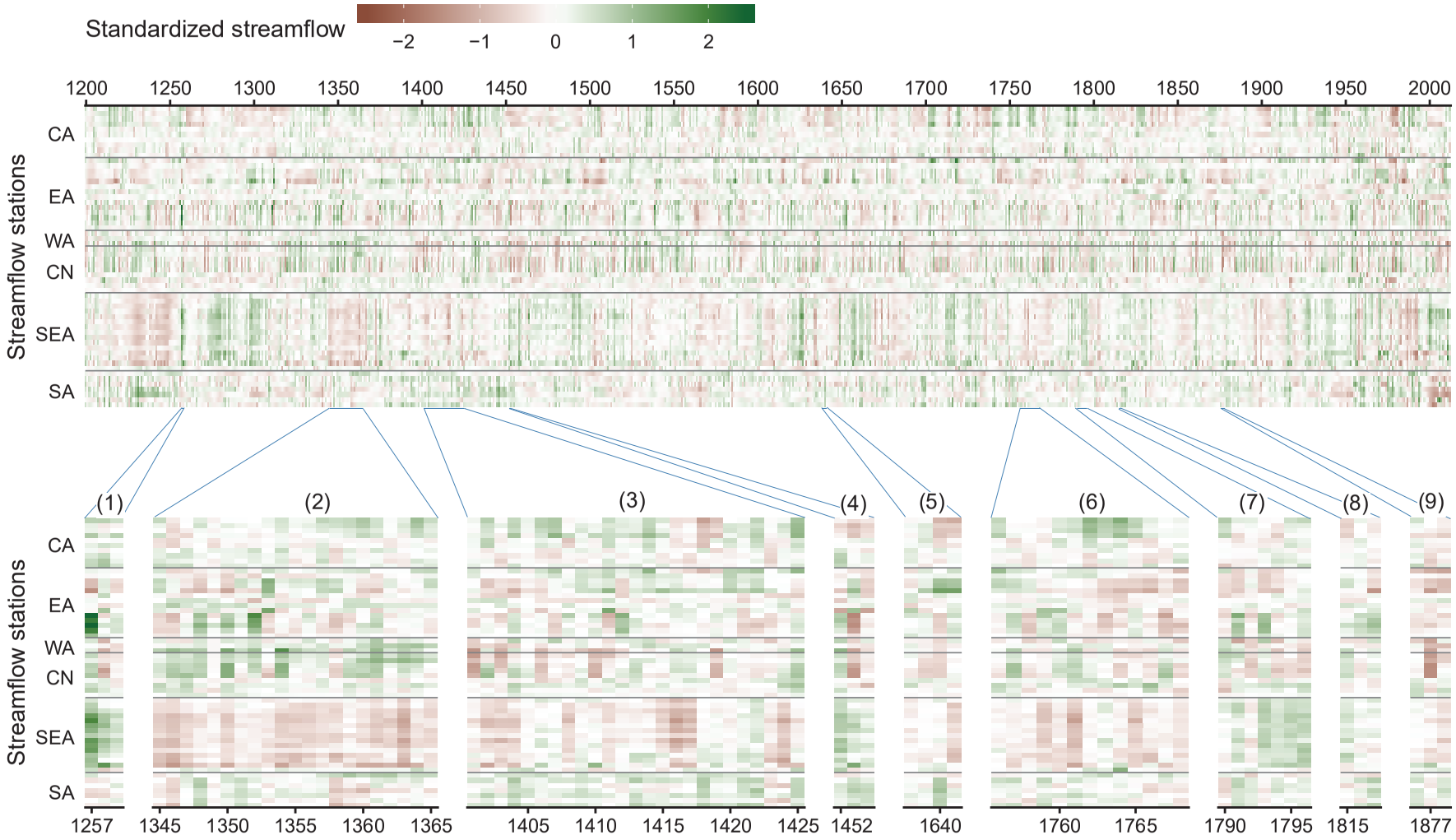

Figure 3. Spatiotemporal variability of streamflow in Asia. a) Variations of the standardized streamflow index (i.e., z-score of the log-transformed streamflow) over time (x-axis) and space (y-axis). The stations are arranged approximately north to south (top down on y-axis) and divided into five regions as delineated in Figure 1: CA (Central Asia), EA (East Asia), WA (West Asia), CN (eastern China), SEA (Southeast Asia), and SA (South Asia). b) Historic events captured in the reconstruction: (1) Samalas eruption, (2) and (3) Angkor Droughts I and II, (4) Kuwae eruption, (5) Ming Dynasty Drought, (6) Strange Parallels Drought, (7) East India Drought, (8) Tambora eruption, and (9) Victorian Great Drought.

1998), these three eruptions saw a persistent streamflow pattern across Southeast Asia, eastern China, and West Asia. In the eruption year t ($t = 1257, 1452, 1815$), abnormally high streamflow occurred in all three regions. In year $t + 1$, streamflow remained high in Southeast Asia but abruptly turned low in West Asia and parts of eastern China. This is unexpected given the results of Li et al. (2013). They found that in year t, PDSI (captured by the MADA) was negative in all three regions; in year $t+1$, PDSI remained negative in Southeast Asia but turned positive in West Asia and eastern China. Based on their findings, one would expect streamflow to be low in all three regions in year t, then remain low in Southeast Asia but turn high in West Asia and eastern China in year $t + 1$. We observe the opposite. Interestingly, Anchukaitis et al. (2010), also using PDSI, found in year t wet conditions in Southeast Asia (similar to our results) but mixed wet and dry conditions in eastern China and West Asia (more similar to Li et al., 2013). The disparity in these studies are attributed to the different sets of eruptions used—Anchukaitis et al. (2010) demonstrated this with three sets of events. Our divergence from their results are partly because they used Superposed Epoch Analysis while we analyze individual events, but we argue that the main cause is streamflow versus PDSI. With our streamflow results, we offer a reconciling explanation: during and immediately after the eruptions, PDSI was more driven by temperature than precipitation, and while low temperature may have caused negative PDSI, it reduced evaporation and consequently, increased streamflow. This mechanism is particularly relevant in midlatitude eastern China and West Asia. In Southeast Asia, however, reduced temperature, from warm to cool, could increase soil moisture (Anchukaitis et al., 2010), resulting in high streamflow. Not disagreeing with previous works, our results offer a look at another aspect of past climate using streamflow instead of PDSI.

As a drought/pluvial indicator, streamflow may differ from PDSI in individual years, as discussed above, but on longer terms, our reconstructed streamflow agrees well with reconstructed PDSI. For example, our record fully captures the Angkor Droughts (1345–1365 and 1401–1425) (Buckley et al., 2010) with prolonged low flow throughout the Mekong and Chao Phraya basins (Southeast Asia). Heavy monsoon rain interrupted these megadroughts; such abrupt alterations to the flow regime proved difficult for Angkor's water managers (Buckley et al., 2014). After the first Angkor Drought, they altered the inflow/outflow functions of their *barays* (reservoirs) in an attempt to preserve water. Heavy rains and flooding subsequently destroyed the reduced-capacity hydraulic infrastructure. Our reconstruction shows that this flood likely occurred in 1375. By the second Angkor Drought, the hydraulic city had insufficient water storage and could not recover. Four more megadroughts that severely affected Asian societies (Cook et al., 2010) are also captured in our reconstruction, along with other major droughts and pluvials. Central Asia observed a six-decade drought between 1260–1320 and sustained pluvials during 1740–1769. Northern Japan experienced extended drought between 1493–1510. Most notably, Southeast Asia suffered a drought between 1226–1249 that was comparable to Angkor Drought I, followed by a multi-decadal pluvial 1271–1307; the drought is prominent in the speleothem record of Wang et al. (2019), and the pluvial can also be traced from there.

3.3 Links to Oceanic Drivers

To exemplify the spatial variation of how the oceans influence streamflow, we selected four river basins from west to east: Krishna, Chao Phraya, Mekong, and Yangtze (Figure 1). We calculated the correlation between reconstructed annual streamflow at each basin and the seasonal averages of global sea surface temperature (SST) for the period 1855–2012. Correlation patterns vary both seasonally and spatially, with differences among rivers and among oceans.

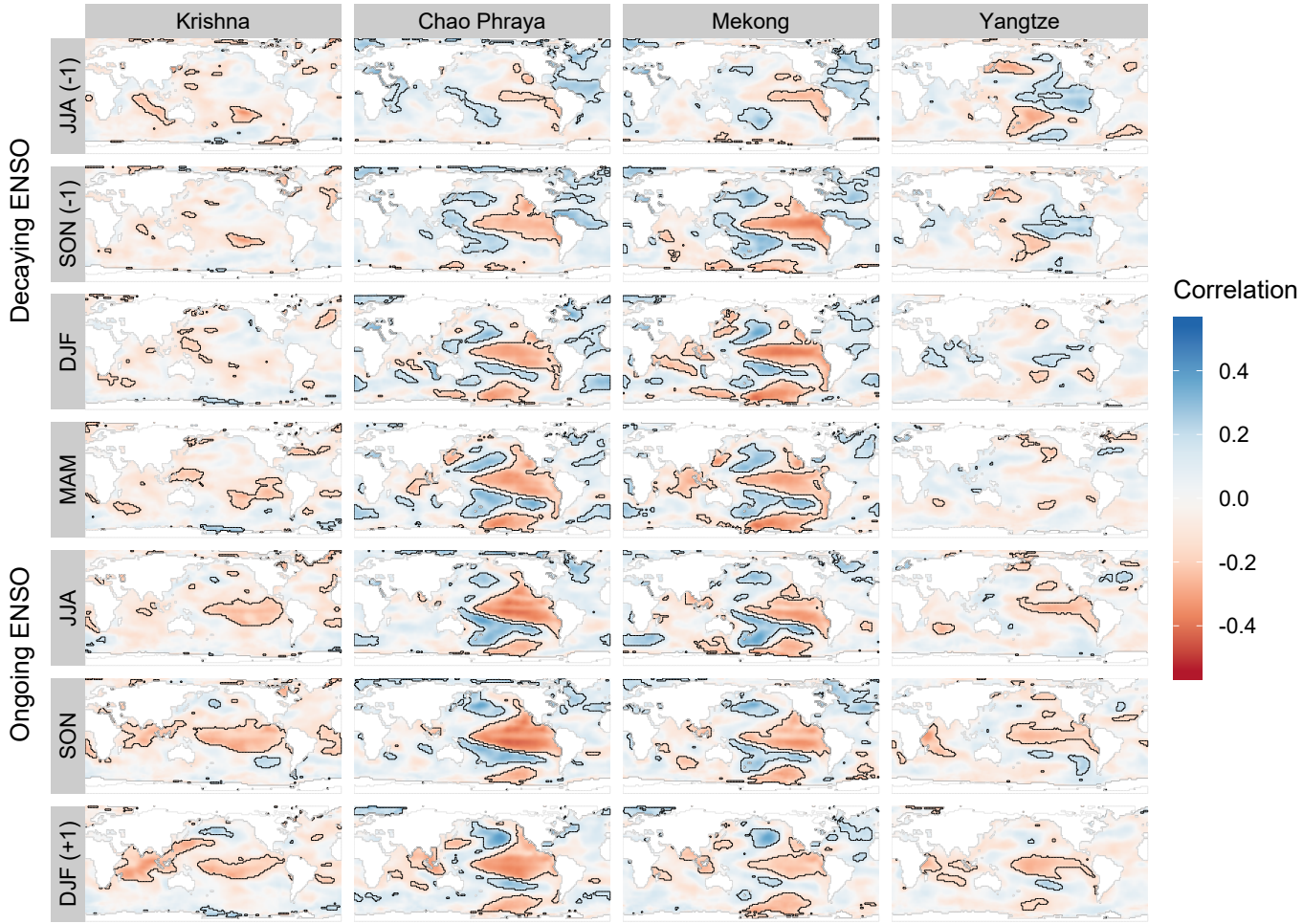

Figure 4. Correlation between reconstructed mean annual streamflow at four river basins (this work) and seasonal averages of global sea surface temperature (SST) from the NOAA_ERSST_v5 data set (Huang et al., 2017) for the period 1855–2012; significant correlations ($\alpha = 0.05$) enclosed in black boundaries. The stations used are shown in Figure S2. "(-1)" denotes previous year.

3.3.1 Pacific Ocean

For the Krishna, significant correlations are mainly observed in the tropical Pacific during summer (JJA) and autumn (SON) of the current year. Tropical Pacific SST—a manifestation of the El Niño-Southern Oscillation (*c.f.* McPhaden et al., 2006)—correlates negatively with streamflow. The hydroclimate of South Asia tends to be drier during El Niños and wetter during La Niñas. These tendencies have also been observed from tree ring records (Borgaonkar et al., 2010), reconstructed PDSI (Yu et al., 2018) and precipitation (Shi and Wang, 2018). The seasonality of correlation suggests that annual streamflow responds more strongly to an ongoing ENSO event than to a decaying one.

The Yangtze has a similar current summer–winter Pacific SST correlation pattern to that of the Krishna (i.e, related to ongoing ENSO events), but it responds to decaying ENSO events (prior summer–winter) more strongly than does the Krishna; correlation with decaying ENSO events takes the opposite sign to that of ongoing ENSO events. These opposite ENSO influences on eastern China have been shown in a similar seasonal correlation analysis using reconstructed precipitation (Shi and Wang, 2018) but not in the annual composite analyses of Yu et al. (2018) and Li et al. (2013). The latter two works showed wetter tendencies during El Niño and drier tendencies during La Niña, likely capturing only the decaying phase.

Unlike in the Krishna and Yangtze, streamflow in the Chao Phraya and Mekong correlates significantly with SST over most of the Pacific Ocean, and the correlation persists across all seasons, reflecting equal influences from decaying and ongoing ENSO events. The basin-wide correlation pattern and its lack of seasonality suggest influences from a driver at longer time scales, likely the Pacific Decadal Variability (PDV)—decadal variations of Pacific SST resulted from complex tropical-extratropical ocean-atmosphere interactions (Henley, 2017). The North Pacific component of PDV is known as the Pacific Decadal Oscillation (PDO) (Mantua and Hare, 2002), its southern counterpart the South Pacific Decadal Oscillation (Shakun and Shaman, 2009); basin-wide SST variation patterns have also been termed Interdecadal Pacific Oscillation (Folland et al., 1999). These modes are closely related (Henley, 2017). The PDO has been shown to influence hydroclimatic variability in Monsoon Asia, in conjunction with ENSO (Yu et al., 2018). Specifically for the Chao Phraya, PDO also modulates ENSO's influence on peak flow (Xu et al., 2019). Here, by juxtaposing the correlation maps, our analyses reveal that ENSO and PDV exert their greatest influence on the Mekong and Chao Phraya.

3.3.2 Indian Ocean

We detect significant negative correlations between streamflow and Indian Ocean SST in current-year fall and winter in the Krishna, Chao Phraya, and Yangtze, and to a lesser extent in the Mekong. These basin-wide correlation patterns follow closely after peak ENSO correlations in summer and fall, consistent with the Indo-Pacific coupling described by Saji et al. (1999): an ENSO event in the Pacific leads to SST anomalies of the same sign in the Indian Ocean. This mode accounts for about 30% of Indian Ocean SST variability [*ibid*]. These authors also proposed another mode—the Indian Ocean Dipole (IOD) mode, the positive phase of which is characterized by cool eastern Indian Ocean around Sumatra, and warm western Indian Ocean around East Africa. Positive IOD events often occur around June–July, peak in October and abruptly end in November, a phenomenon called seasonal locking (Saji et al., 1999; Ummenhofer et al., 2017). Positive IOD events have been linked to droughts in Southeast Asia but this relationship is not robust (Ummenhofer et al., 2013). Consistent with their results, we observe an east-positive–west-negative correlation pattern between Indian Ocean SST and Southeast Asia streamflow (Mekong and Chao Phraya) in prior year fall (the peak IOD season), with small areas of significant correlation. This pattern is not clear in present-year fall, likely because it is dominated by the basin-wide ENSO mode (the IOD mode only accounts for 12% of Indian Ocean SST variability (Saji et al., 1999)).

3.3.3 Atlantic Ocean

The Chao Phraya and Mekong streamflow correlates positively with tropical and North Atlantic SST, with significant correlations observed throughout the seasons. Wang et al. (2019) proposed a mechanism to explain this relationship: increased tropical Atlantic SST leads to changes in zonal moisture transport, causing depression over tropical Indian Ocean, reducing rainout over the basin, leaving more moisture available to be transported to mainland Southeast Asia, ultimately strengthen Indian Monsoon rain over the Mekong and Chao Phraya. The reduced upstream rainout may also contribute to decreased streamflow in the Krishna, which lies upstream of the Chao Phraya and Mekong in the moisture transport path (*c.f.* Buckley et al., 2014, Figure 13). Hence, the mechanism of Wang et al. (2019) is also consistent with the negative correlation between tropical Atlantic SST and Krisha's streamflow.

3.4 Implications for water management

From our reconstruction, streamflow in Monsoon Asia appears coherent: high and low flows often occur simultaneously at nearby gauges and adjacent basins (Figure 3). This emerges even though we reconstructed each gauge individually, proving the merits of point-by-point regression.

More importantly, this coherence implies that water management in Asia should be coordinated among basins. For example, Thailand is increasingly purchasing Mekong-generated hydropower from Laos, and when that is insufficient, complements its energy needs with thermal power from plants that use water from the Chao Phraya for cooling (Chowdhury et al., 2019). Thailand's energy system is at risk when a prolonged drought occurs at both rivers—our record shows such events have happened several times in the past (Figure 3).

We showed that the Pacific, Indian, and Atlantic Oceans contribute to streamflow variability (frequency analyses further corroborate this, see Text S3). Therefore, water management in Monsoon Asia should take into account the ocean states. A case study of the Angat River, the Philippines, showed that reservoir operating policies informed by ENSO states are more robust than conventional policies (Libisch-Lehner et al., 2019). Operating policies may be improved further if, say, the PDV is also considered.

4 Conclusions

Using a novel climate-informed dynamic reconstruction algorithm and the Monsoon Asia Drought Atlas as the climate proxy, we reconstructed eight centuries of streamflow at 63 stations in 16 countries across Monsoon Asia. The algorithm is skillful over 92% of the stations; skill distribution is spatially homogeneous. Our reconstruction shows that streamflow in Monsoon Asia is spatially coherent, with concurrent high/low flow episodes in adjacent basins. This coherence is attributed to common oceanic drivers—the El Niño–Southern Oscillation, the Pacific Decadal Variability, the Indian Ocean Dipole, and tropical Atlantic sea surface temperature variations. These oceanic drivers exert their greatest influences on the Mekong and Chao Phraya basins. Our results suggest that water resources management in Monsoon Asia be coordinated among basins, and shed some light on the potential for improving water management by observing the ocean states. These insights may benefit the riparian people of Monsoon Asia.

Acknowledgments

Hung Nguyen is supported by the President's Graduate Fellowship from the Singapore University of Technology and Design. We thank Edward Cook, Caroline Ummenhofer, Nerilie Abram, Nathalie Goodkin, and Xun Sun for insightful comments. We are grateful to Thanh Dang, Mukund Rao, Rosanne D'Arrigo, Donghoon Lee, and Caroline Leland for streamflow data of the Mekong, Brahmaputra, Citarum, Han, and Yeruu Rivers. Chao Phraya River data were obtained from the Thai Royal Irrigation Department at `www.hydro1.net`, Indus River from Rao et al. (2018, Supporting Information), other streamflow data from GSIM (Do et al., 2018; Gudmundsson et al., 2018), MADA v2 data from Marvel et al. (2019) at `www.dropbox.com/s/n2lo99h9qn17prg/madaV2.nc`, river network data from FLO1K (Barbarossa et al., 2018) with help postprocessing by Valerio Barbarossa, basin boundary data from HydroSHEDS (Lehner and Grill, 2013) at `hydrosheds.org`, SST data from NOAA ERSST v5 (Huang et al., 2017) provided by the NOAA/OAR/ESRL PSD, Boulder, Colorado, USA, at `www.esrl.noaa.gov/psd/`. This work was conducted with open-source software: analysis and visualization performed in R and manuscript written in LaTeX. We thank the open-source software community, especially the R package creators and maintainers, for their contributions to open science. Data and code necessary to reproduce the results are available at `https://github.com/ntthung/paleo-asia`, except instrumental data of the Mekong, Yangtze, and Pearl rivers due to restrictions. (If this work is accepted, we shall also upload all reconstruction results to NOAA.) Lamont contribution number XXXX.

References

Anchukaitis, K. J., Buckley, B. M., Cook, E. R., Cook, B. I., D'Arrigo, R. D., and Ammann, C. M. (2010). Influence of volcanic eruptions on the climate of the Asian monsoon region. *Geophysical Research Letters*, 37(22):1–5.

Barbarossa, V., Huijbregts, M. A., Beusen, A. H., Beck, H. E., King, H., and Schipper, A. M. (2018). FLO1K, global maps of mean, maximum and minimum annual streamflow at 1 km resolution from 1960 through 2015. *Scientific Data*, 5(October 2017):180052.

Best, J. (2019). Anthropogenic stresses on the world's big rivers. *Nature Geoscience*, 12(1):7–21.

Boers, N., Goswami, B., Rheinwalt, A., Bookhagen, B., Hoskins, B., and Kurths, J. (2019). Complex networks reveal global pattern of extreme-rainfall teleconnections. *Nature*.

Borgaonkar, H. P., Sikder, A. B., Ram, S., and Pant, G. B. (2010). El Niño and related monsoon drought signals in 523-year-long ring width records of teak (Tectona grandis L.F.) trees from south India. *Palaeogeography, Palaeoclimatology, Palaeoecology*, 285(1-2):74–84.

Briffa, K. R., Jones', P. D., Schweingruber, F. H., and Osborn, T. J. (1998). Influence of volcanic eruptions on Northern Hemisphere summer temperature over the past 600 years. *Nature*, 393(6684):450–455.

Buckley, B. M., Anchukaitis, K. J., Penny, D., Fletcher, R., Cook, E. R., Sano, M., Nam, L. C., Wichienkeeo, A., Minh, T. T., and Hong, T. M. (2010). Climate as a contributing factor in the demise of Angkor, Cambodia. *Proceedings of the National Academy of Sciences*, 107(15):6748–6752.

Buckley, B. M., Fletcher, R., Wang, S. Y. S., Zottoli, B., and Pottier, C. (2014). Monsoon extremes and society over the past millennium on mainland Southeast Asia. *Quaternary Science Reviews*, 95:1–19.

Buckley, B. M., Palakit, K., Duangsathaporn, K., Sanguantham, P., and Prasomsin, P. (2007). Decadal scale droughts over northwestern Thailand over the past 448 years: Links to the tropical Pacific and Indian Ocean sectors. *Climate Dynamics*, 29(1):63–71.

Chowdhury, A. F. M. K., Dang, D. T., and Galelli, S. (2019). Impacts of Hydro-climatic Variability on the Energy System of the Greater Mekong Sub-region.

Cook, E. R. (2015). Developing MADAv2 Using The Point-By-Point Regression Climate Field Reconstruction Method.

Cook, E. R., Anchukaitis, K. J., Buckley, B. M., D'Arrigo, R. D., Jacoby, G. C., and Wright, W. E. (2010). Asian Monsoon Failure and Megadrought During the Last Millennium. *Science*, 328(5977):486–489.

Cook, E. R. and Kairiukstis, L. A. (1990). *Methods of dendrochronology. Applications in the Environmental Sciences*. Kluwer Academic Publishers.

Cook, E. R., Meko, D. M., Stahle, D. W., and Cleaveland, M. K. (1999). Drought Reconstructuions for the continental United States. *Journal of Climate*, 12(APRIL):1145–1162.

D'Arrigo, R., Abram, N., Ummenhofer, C., Palmer, J., and Mudelsee, M. (2011). Reconstructed streamflow for Citarum River, Java, Indonesia: linkages to tropical climate dynamics. *Climate Dynamics*, 36(3-4):451–462.

Davi, N. K., Jacoby, G. C., Curtis, A. E., and Baatarbileg, N. (2006). Extension of drought records for central Asia using tree rings: West-central Mongolia. *Journal of Climate*, 19(1):288–299.

Davi, N. K., Pederson, N., Leland, C., Nachin, B., Suran, B., and Jacoby, G. C. (2013). Is eastern Mongolia drying? A long-term perspective of a multidecadal trend. *Water Resources Research*, 49(1):151–158.

Do, H. X., Gudmundsson, L., Leonard, M., and Westra, S. (2018). The Global Streamflow Indices and Metadata Archive (GSIM) – Part 1: The production of a daily streamflow archive and metadata. *Earth System Science Data*, 10(2):765–785.

Folland, C. K., Parker, D. E., Colman, A. W., and Washington, R. (1999). Large Scale Modes of Ocean Surface Temperature Since the Late Nineteenth Century. In *Beyond El Niño*, pages 73–102. Springer Berlin Heidelberg, Berlin, Heidelberg.

Gao, C., Robock, A., Self, S., Witter, J. B., Steffenson, J. P., Clausen, H. B., Siggaard-Andersen, M. L., Johnsen, S., Mayewski, P. A., and Ammann, C. (2006). The 1452 or 1453 A.D. Kuwae eruption signal derived from multiple ice core records: Greatest volcanic sulfate event of the past 700 years. *Journal of Geophysical Research Atmospheres*, 111(12):1–11.

Gudmundsson, L., Do, H. X., Leonard, M., and Westra, S. (2018). The Global Streamflow Indices and Metadata Archive (GSIM) – Part 2: Quality control, time-series indices and homogeneity assessment. *Earth System Science Data*, 10(2):787–804.

Henley, B. J. (2017). Pacific decadal climate variability: Indices, patterns and tropical-extratropical interactions. *Global and Planetary Change*, 155(October 2016):42–55.

Ho, M., Lall, U., and Cook, E. R. (2016). Can a paleodrought record be used to reconstruct streamflow?: A case study for the Missouri River Basin. *Water Resources Research*, 52(7):5195–5212.

Ho, M., Lall, U., Sun, X., and Cook, E. R. (2017). Multiscale temporal variability and regional patterns in 555 years of conterminous U.S. streamflow. *Water Resources Research*, 53(4):3047–3066.

Huang, B., Thorne, P. W., Banzon, V. F., Boyer, T., Chepurin, G., Lawrimore, J. H., Menne, M. J., Smith, T. M., Vose, R. S., and Zhang, H.-M. (2017). Extended Reconstructed Sea Surface Temperature, Version 5 (ERSSTv5): Upgrades, Validations, and Intercomparisons. *Journal of Climate*, 30(20):8179–8205.

Knoben, W. J. M., Woods, R. A., and Freer, J. E. (2018). A Quantitative Hydrological Climate Classification Evaluated With Independent Streamflow Data. *Water Resources Research*, 54(7):5088–5109.

Lavigne, F., Degeai, J. P., Komorowski, J. C., Guillet, S., Robert, V., Lahitte, P., Oppenheimer, C., Stoffel, M., Vidal, C. M., Suronoh, Pratomo, I., Wassmer, P., Hajdas, I., Hadmoko, D. S., and De Belizal, E. (2013). Source of the great A.D. 1257 mystery eruption unveiled, Samalas volcano, Rinjani Volcanic Complex, Indonesia. *Proceedings of the National Academy of Sciences of the United States of America*, 110(42):16742–16747.

Lehner, B. and Grill, G. (2013). Global river hydrography and network routing: baseline data and new approaches to study the world's large river systems. *Hydrological Processes*, 27(15):2171–2186.

Li, J., Xie, S.-P., Cook, E. R., Chen, F., Shi, J., Zhang, D. D., Fang, K., Gou, X., Li, T., Peng, J., Shi, S., and Zhao, Y. (2019). Deciphering Human Contributions to Yellow River Flow Reductions and Downstream Drying Using Centuries-Long Tree Ring Records. *Geophysical Research Letters*, 46(2):898–905.

Li, J., Xie, S.-p., Cook, E. R., Morales, M. S., Christie, D. A., Johnson, N. C., Chen, F., D'Arrigo, R., Fowler, A. M., Gou, X., and Fang, K. (2013). El Niño modulations over the past seven centuries. *Nature Climate Change*, 3(9):822–826.

Libisch-Lehner, C. P., Nguyen, H. T., Taormina, R., Nachtnebel, H. P., and Galelli, S. (2019). On the Value of ENSO State for Urban Water Supply System Operators: Opportunities, Trade-Offs, and Challenges. *Water Resources Research*, pages 1–20.

Mantua, N. J. and Hare, S. R. (2002). The Pacific Decadal Oscillation. *Journal of Oceanography*, 58(1):35–44.

Marvel, K., Cook, B. I., Bonfils, C. J. W., Durack, P. J., Smerdon, J. E., and Williams, A. P. (2019). Twentieth-century hydroclimate changes consistent with human influence. *Nature*, 569(7754):59–65.

McPhaden, M. J., Zebiak, S. E., and Glantz, M. H. (2006). ENSO as an Integrating Concept in Earth Science. *Science*, 314(5806):1740–1745.

Nguyen, H. T. T. and Galelli, S. (2018). A Linear Dynamical Systems Approach to Streamflow Reconstruction Reveals History of Regime Shifts in Northern Thailand. *Water Resources Research*, 54(3):2057–2077.

Palmer, W. C. (1965). *Meteorological Drought. Research Paper No. 45.* U.S. Department of Commerce Weather Bureau.

Pederson, N., Hessl, A. E., Baatarbileg, N., Anchukaitis, K. J., and Di Cosmo, N. (2014). Pluvials, droughts, the Mongol Empire, and modern Mongolia. *Proceedings of the National Academy of Sciences of the United States of America*, 111(12):4375–4379.

Pederson, N., Leland, C., Nachin, B., Hessl, A. E., Bell, A. R., Martin-Benito, D., Saladyga, T., Suran, B., Brown, P. M., and Davi, N. K. (2013). Three centuries of shifting hydroclimatic regimes across the Mongolian Breadbasket. *Agricultural and Forest Meteorology*, 178-179:10–20.

Pelletier, J. D. and Turcotte, D. L. (1997). Long-range persistence in climatological and hydrological time series: Analysis, modeling and application to drought hazard assessment. *Journal of Hydrology*, 203(1-4):198–208.

Rao, M. P., Cook, E. R., Cook, B. I., Palmer, J. G., Uriarte, M., Devineni, N., Lall, U., D'Arrigo, R. D., Woodhouse, C. A., Ahmed, M., Zafar, M. U., Khan, N., Khan, A., and Wahab, M. (2018). Six Centuries of Upper Indus Basin Streamflow Variability and Its Climatic Drivers. *Water Resources Research*, 54(8):5687–5701.

Saji, N. H., Goswami, B. N., Vinayachandran, P. N., and Yamagata, T. (1999). A dipole mode in the tropical Indian Ocean. *Nature*, 401(6751):360–363.

Sano, M., Buckley, B. M., and Sweda, T. (2009). Tree-ring based hydroclimate reconstruction over northern Vietnam from Fokienia hodginsi: Eighteenth century mega-drought and tropical Pacific influence. *Climate Dynamics*, 33(2-3):331–340.

Shakun, J. D. and Shaman, J. (2009). Tropical origins of North and South Pacific decadal variability. *Geophysical Research Letters*, 36(19):L19711.

Shi, H. and Wang, B. (2018). How does the Asian summer precipitation-ENSO relationship change over the past 544 years? *Climate Dynamics*, 0(0):0.

Sigl, M., Winstrup, M., McConnell, J. R., Welten, K. C., Plunkett, G., Ludlow, F., Büntgen, U., Caffee, M., Chellman, N., Dahl-Jensen, D., Fischer, H., Kipfstuhl, S., Kostick, C., Maselli, O. J., Mekhaldi, F., Mulvaney, R., Muscheler, R., Pasteris, D. R., Pilcher, J. R., Salzer, M., Schüpbach, S., Steffensen, J. P., Vinther, B. M., and Woodruff, T. E. (2015). Timing and climate forcing of volcanic eruptions for the past 2,500 years. *Nature*, 523(7562):543–549.

Stockton, C. and Jacoby, G. C. (1976). Long-term Surface-water Supply and Streamflow Trends in the Upper Colorado River Basin Based on Tree-ring Analyses. Technical report, Lake Powell Research Project.

Stothers, R. B. (1984). The Great Tambora Eruption in 1815 and Its Aftermath. *Science*, 224(4654):1191–1198.

Turner, S. W. D. and Galelli, S. (2016). Regime-shifting streamflow processes: Implications for water supply reservoir operations. *Water Resources Research*, 52(5):3984–4002.

Ummenhofer, C. C., Biastoch, A., and Böning, C. W. (2017). Multidecadal indian ocean variability linked to the pacific and implications for preconditioning indian ocean dipole events. *Journal of Climate*, 30(5):1739–1751.

Ummenhofer, C. C., D'Arrigo, R. D., Anchukaitis, K. J., Buckley, B. M., and Cook, E. R. (2013). Links between Indo-Pacific climate variability and drought in the Monsoon Asia Drought Atlas. *Climate Dynamics*, 40(5-6):1319–1334.

Wang, J. K., Johnson, K. R., Borsato, A., Amaya, D. J., Griffiths, M. L., Henderson, G. M., Frisia, S., and Mason, A. (2019). Hydroclimatic variability in Southeast Asia over the past two millennia. *Earth and Planetary Science Letters*, 525:115737.

Woodhouse, C. A., Gray, S. T., and Meko, D. M. (2006). Updated streamflow reconstructions for the Upper Colorado River Basin. *Water Resources Research*, 42(5):1–16.

Xu, C., Buckley, B. M., Promchote, P., Wang, S. S., Pumijumnong, N., An, W., Sano, M., Nakatsuka, T., and Guo, Z. (2019). Increased Variability of Thailand's Chao Phraya River Peak Season Flow and Its Association With ENSO Variability: Evidence From Tree Ring δ ¹⁸ O. *Geophysical Research Letters*, page 2018GL081458.

Yu, E., King, M. P., Sobolowski, S., Otterå, O. H., and Gao, Y. (2018). Asian droughts in the last millennium: a search for robust impacts of Pacific Ocean surface temperature variabilities. *Climate Dynamics*, 50(11-12):4671–4689.